Analysis of Groundwater Recharge in Mongolian Drylands Using Composite Vadose Zone Modeling

Khulan Batsukh[1†], Vitaly A. Zlotnik[1†] and Paolo Nasta[2†]*

[1] *Department of Earth and Atmospheric Sciences, University of Nebraska-Lincoln, Lincoln, NE, United States,* [2] *Department of Agricultural Sciences, University of Naples Federico II, Naples, Italy*

Knowledge of groundwater recharge (*GR*) is important for the effective management of water resources under semi-arid continental climates. Unfortunately, studies and data in Mongolia are limited due to the constraints in funding and lack of research infrastructures. Currently, the wide accessibility of freely available global-scale digital datasets of physical and chemical soil properties, weather data, vegetation characteristics, and depths to the water table offers new tools and basic information that can support low-cost physically based and process-oriented models. Estimates of *GR* over 41 study sites in Mongolia were obtained using HYDRUS-1D in a 2-m-thick soil profile with root depths of either 0.30 or 0.97 m by exploiting the daily precipitation and biome-specific potential evapotranspiration values. The *GR* simulated by HYDRUS-1D arrives at the water table and becomes the actual *GR* with a lag time that has been calculated using a simplified form of the Richards equation and a traveling wave model. The mean annual precipitation ranges from 57 to 316 mm year^{-1}, and on average about 95% of it is lost by mean annual actual evapotranspiration. In the steppe region, the vegetation cover induces higher-than-normal actual transpiration losses and consequently lower *GR*. The mean annual *GR* rates span between 0.3 and 12.0 mm year^{-1}, while travel times range between 4 and 558 years. Model prediction uncertainty was quantified by comparing actual evapotranspiration and *GR* with available maps and by a sensitivity assessment of lag time to the soil moisture in the deep vadose zone. The partial least squares regression (PLSR) was used to evaluate the impact of available environmental properties in explaining the 47.1 and 59.1% variability of the spatially averaged mean annual *GR* and travel time, respectively. The most relevant contributors are clay content, aridity index, and leaf area index for *GR*, and depth to the water table and silt content for the lag time. In data-poor, arid, and semi-arid regions such as Mongolia, where the mean annual *GR* rates are low and poorly correlated to precipitation, the ever-increasing availability of world databases and remote sensing products offers promise in estimating *GR*.

Keywords: HYDRUS-1D, soil moisture, lag time, Rosetta, semi-arid climate, partial least squares regression (PLSR)

INTRODUCTION

Groundwater is a vital ecosystem service in arid and semi-arid regions where the surface water resources are generally scarce and highly unreliable, especially under the increasing number of projected drought events induced by climate change (Deng et al., 2015). Therefore, sustainable management of water resources relies on the accurate assessment of low annual groundwater recharge (GR) rates that nevertheless are significant in a vast territory such as Mongolia. Direct measurements of GR like lysimeters are unfeasible because they involve costly, time-consuming, and labor-intensive efforts (Lerner et al., 1990; Jyrkama et al., 2002; Scanlon et al., 2002). More affordable field approaches based on chloride mass balance are commonly used to estimate GR in regions with similar environmental characteristics, e.g., Inner Mongolia, China (Gates et al., 2008; Yin et al., 2011; Deng et al., 2015; Huang et al., 2017). However, these approaches have not been used yet in Mongolia, to our knowledge.

The main available source on renewable groundwater resources in Mongolia was published by Jadambaa et al. (2012, Figures A1–71). The "renewable resources" include both diffuse and focused recharge plus lateral inflow (here, definitions of diffuse and focused recharge follow Lerner et al., 1990 and Healy, 2011). Results are largely based on the hydrograph separation method and provide the only material relevant to groundwater recharge assessment. According to this map, 76% of the country has groundwater renewable resources of <10 mm year^{-1}, and 84% of the country has groundwater renewable resources of <20 mm year^{-1}. These low values indicate the prevalence of areas with diffuse recharge (Healy, 2011; Meixner et al., 2016). Higher GR rates due to focused recharge are reported in river catchments, where runoff generated by snowpack in mountainous areas serves as the water source for GR in topographic depressions with extensive surface water–groundwater exchange. However, there is a clear understanding that "…so far more detailed estimation of groundwater resources of Mongolia has yet to be done" as reported in Gombo and Dambaravjaa (2012, p. 23). According to the mean annual groundwater recharge map of the world (WaterGAP 2.1, University of Frankfurt/Main; modified by WHYMAP, B., 2008), groundwater recharge is <20 mm year^{-1} in most parts of the country.

Currently, the accessibility of freely available global-scale digital datasets of soil physical and chemical properties, weather data, leaf area indexes, root zone depths, and depths to water table opens new opportunities in providing low-cost basic information that can support physically based and process-oriented models (Zlotnik et al., 2016; Doble and Crosbie, 2017; Pozdniakov et al., 2020). These models simulate the water balance in the groundwater–soil–plant–atmosphere system and probably represent the most promising affordable methods in Mongolia (Bayanzul et al., 2019). Feeding these models with robust input data allows the modeler to establish relationships among groundwater recharge, precipitation, and evapotranspiration, influenced by vegetation, local topography, soil hydraulic properties, and groundwater depth (e.g., Scanlon et al., 2002;

Crosbie et al., 2013). These numerical simulations can be supplemented by simplified approaches to estimate soil moisture travel time across the deep vadose zone.

Therefore, the objectives of the study are as follows:

- quantification of drainage (assumed as potential groundwater recharge, GR_p) from a 2-m-thick soil profile (shallow vadose zone) by using HYDRUS-1D;
- evaluation of the consistency of our results with available maps of GR_p and actual evapotranspiration (ET_a) provided by the Regional Hydrogeological Map of Mongolia and Food And Agriculture Organization (FAO), respectively;
- calculation of the lag (travel) time of actual groundwater recharge, GR_a, between the shallow vadose zone bottom (2-m depth) and the water table; GR_a is assumed to be equal to GR_p.

This proposed composite low-cost methodology has practical significance for Mongolia in the absence of ground truth measurements. The renewable groundwater resources map is a primary available data source for water resource planning in Mongolia. However, other studies ignore GR or fail to use recent methodologies. Previously, GR was often neglected in Mongolia or methods failed to consider various factors influencing GR. Our method helps understand GR dynamics in several locations with different vegetation characteristics, precipitation regime, and soil properties. Most importantly, the site-specific groundwater recharge results can be exploited for supporting sustainable management of water resources and can be the basis for future studies.

MATERIALS AND METHODS

Study Area and Available Data

Mongolia is a landlocked territory of 1,564,116 km^2 in the heart of the Asian continent on a high plateau surrounded by mountain ridges, in the transition zone between the Siberian taiga and the dry steppes and semi-deserts of central Asia. The country has a distinctly dry subarctic continental climate, with long cold winters and short hot summers. The mean annual precipitation in Mongolia is about 200 mm year^{-1}, ranging from <50 mm year^{-1} in the Gobi Desert region to over 500 mm year^{-1} in the mountainous regions in the north. Maximum seasonal precipitation occurs in the summer (Yu et al., 2016).

About half of the Mongolian territory is mountainous with an average elevation of 1,580 m a.s.l.; about 81% of its territory is above 1,000 m and 19% below 1,000 m (Yembuu, 1906). These mountains are divided into cool and dry types according to their vertical vegetation range. The Khentii, Khuvsgul, northwestern Mongolian Altai, Northern Khangai, and Khyangan mountains are cool types and are covered with steppe vegetation of the lower range. The Southern Altai, Gobi Altai, Gobi, and Zuungar mountains are of the dry type with desert vegetation and high-cold steppe (Indree, 2014). The steppe ecosystems are associated with the semi-arid and arid continental temperate climates of the region and are ecologically fragile and sensitive to climate change and anthropogenic disturbances (Li et al., 2007). Perennial plants (50–90%) dominate the Mongolian steppe. The highest

percentage of perennial plants occurs in the high-cold steppe. In contrast, the percentage of shrub, dwarf shrub, biennials, and annuals is minimum in the high-cold steppe and gradually increases in the desert steppe (Indree, 2014). About 80% of the territory is covered by pasture land, 10% by forest, 1% by farmland, and 9% by other land cover types. Steppe vegetation occupies about 83% of the territory (Indree, 2014).

A number of meteorological and other datasets are needed to feed the vadose zone model and for the calculation of vadose zone lag time. The data have been collected from various sources in order to fulfill the lack of *in situ* measurements. The daily precipitation data have been acquired from NAMEM for the 2007–2011 study period. The daily grass-reference potential evapotranspiration, ET_0, was calculated by using the temperature-based Hargreaves method (Batsukh et al., 2021). According to the FAO, the Aridity Index (*AI*) is computed as the ratio between mean annual precipitation and ET_0 and will be used in our study to determine climate classes (Spinoni et al., 2015). A daily crop coefficient, K_c, was used to convert ET_0 into the biome-specific potential evapotranspiration, ET_p, according to the protocol used by Batsukh et al. (2021). Potential evaporation, E_p, and potential transpiration, T_p, were obtained from ET_p by using the time-variant leaf area index (*LAI*) maps based on remote-sensing products (Batsukh et al., 2021). There are no permanent stations for measuring ET_a in Mongolia. In this study, we use an available map of ET_a provided by FAO (2009) to test and validate our model simulations. In general, the mean annual groundwater recharge rate in Mongolia is low especially in the southern parts; it is entirely neglected when this component of the water budget is compared to precipitation (e.g., Nandintsetseg et al., 2010). The main study related to the groundwater recharge in Mongolia by Jadambaa et al. (2012) is based historically and methodologically on the "Regional Hydrogeological Map of Mongolia, Multi-year Mean Flow of Surface Water and Groundwater (Regional Hydrogeologic Map of Mongolia, Multi-year Mean Flow of Surface Water and Groundwater, 1981)" at the scale of 1:1,000,000. The map shows the surface water runoff as contours and the groundwater flow as polygons. The groundwater flow polygons represent the total flow that originates from lateral groundwater flow, infiltration of surface water, and precipitation and are presented in mm year^{-1}. Using data from stream gauging, spring analyses, aquifer characteristics, and borehole information, the Renewable Groundwater Resource Map (Jadambaa et al., 2012, Figures A1–74) was developed by hydrograph separation and used over 40 years for state planning, but *GR* concept was never used. The renewable groundwater resources (*GR* and lateral inflow) represented on the Renewable Groundwater Resource Map have been explained as dependent on precipitation, the hydraulic connection between surface water and groundwater, and groundwater flow from adjacent areas. The legend presents a classification of the natural resources per 1 km^2 as follows: <5, 5–10, 10–20, 20–50, 50–100, 100–200, and >200 mm year^{-1} (Jadambaa et al., 2012, p. 305).

It is worth noticing that in the north and in the mountainous regions, the density of streams increases together with the natural groundwater resources (Jadambaa et al., 2012, p. 20, Figure 1 and

p. 23, Figure 2). Low density of streams in the southern part are signs of the negligible contribution of focused recharge into *GR*, which is low itself.

The depth to water table data in our study locations were obtained from available hydrogeological maps (Mineral Resources and Petroleum Authority, 1994) with substantial uncertainty. The unknown depths to the water table in some locations are approximated as 10 m.

Due to the absence of *in situ* measurements of soil hydraulic parameters, the pedotransfer functions (PTFs) are used to get soil hydraulic parameters from soil physical properties in the study locations (Nasta et al., 2021). In these locations, the most reliable source is Soilgrids250m (van den Bosch and Batjes, 2013; Hengl et al., 2017), and therefore, this data product was used in our study. SoilGrids250m is a system of global digital soil mapping based on state-of-the-art machine learning methods to map the spatial distribution of soil properties across the globe. Sand (%), silt (%), clay (%) content, and bulk density (BD, expressed in kg m^{-3}) have been obtained in six functional layers (0–0.05, 0.05–0.15, 0.15–0.30, 0.30–0.60, 0.60–1.0, and 1–2 m) up to 2-m depth (https://soilgrids.org/). The soil physical and hydraulic properties pertaining to the sixth layer were assumed for the deep vadose zone between the soil depth of 2 m and depth to water table. SoilGrids250m prediction models are fitted using over 230,000 soil profile observations from the WoSIS database and a series of environmental covariates. The outputs of SoilGrids250m are global soil property maps at six standard depth intervals (according to the GlobalSoilMap International Union of Soil Sciences working group and its specifications) at a horizontal spatial resolution of 250 m. Prediction uncertainty is quantified by the lower and upper limits of a 90% prediction interval (van den Bosch and Batjes, 2013).
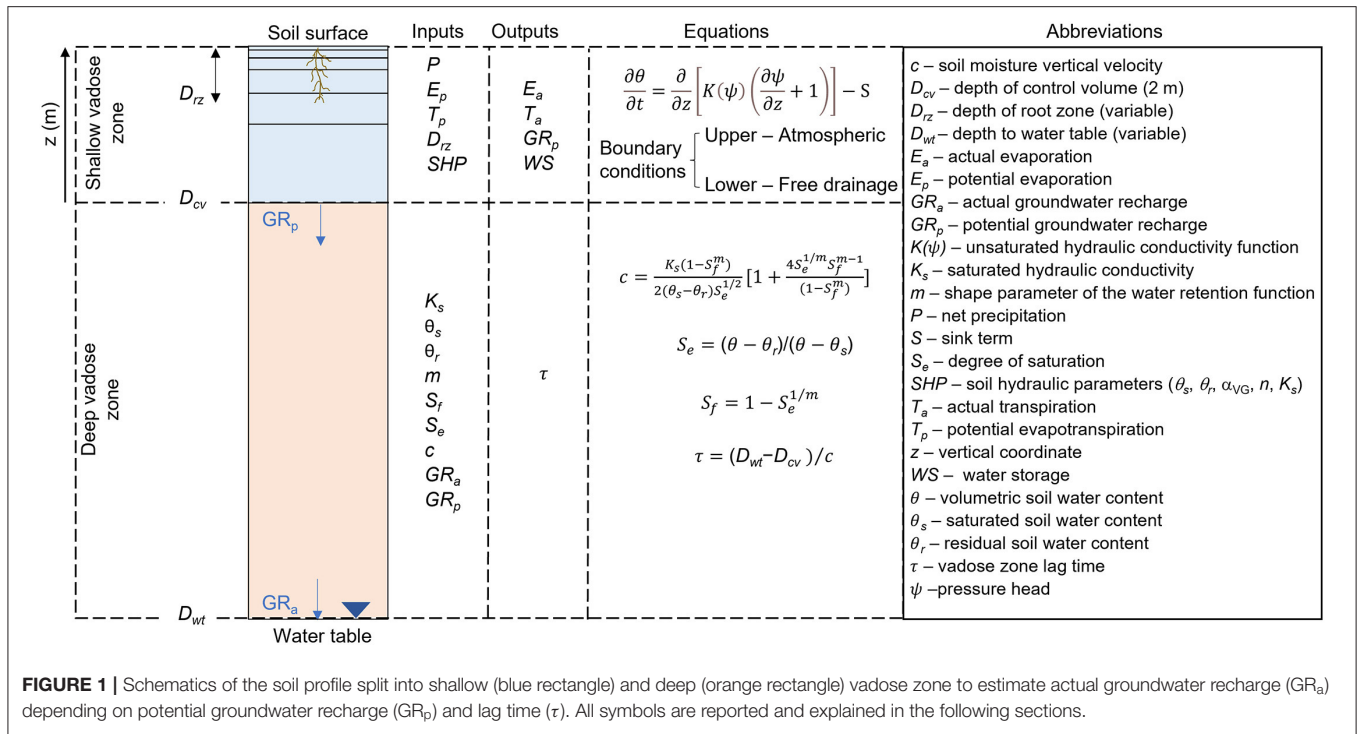
Yanagawa et al. (2015) identified a 0.50-m-thick soil layer in Mongolia as the predominant root zone. Some of the species present in the study area have a well-developed root system, such as *Haloxylon ammodendron*, *Nitraria sphaerocarpa,* and less often *Tamarix ramosissima*. In our study, Ekhiin gol and Tooroi locations are covered by *Haloxylon ammodendron*; thus, a root depth of 0.97 m has been set for this specific vegetation according to Wang et al. (2017). The root zone in other study locations was considered as a 0.30-m-thick soil layer.

Methodology
Model Conceptualization

Precipitation is partly intercepted by vegetation and partially lost by the runoff. Infiltrating water is transpired by plant roots, evaporated from the soil surface, and drained downward below the root zone. GR_p is assumed as the infiltrated water past the root zone (drainage). GR_a is assumed equal to GR_p after soil moisture traverses the vadose zone toward the water table (Crosbie et al., 2010). Our study estimates the recharge at plot scale in 41 experimental locations in Mongolia by setting up a soil profile, which separates the soil surface from the depth to water table.

The soil profile (**Figure 1**) is split into a layered shallow vadose zone delimited by the blue rectangle from soil surface up to the soil depth of 2 m and a uniform deep vadose zone (orange rectangle from soil depth of 2 m up to depth to

FIGURE 1 | Schematics of the soil profile split into shallow (blue rectangle) and deep (orange rectangle) vadose zone to estimate actual groundwater recharge (GR$_a$) depending on potential groundwater recharge (GR$_p$) and lag time (τ). All symbols are reported and explained in the following sections.

the water table). The shallow vadose zone is assumed as the operational water mass control volume. HYDRUS-1D is used to simulate water flow across the shallow vadose zone and estimate GR_p assumed as drainage at the soil depth of 2 m (D_{cv}) under specific soil, vegetation, and climate conditions (Wang et al., 2009). The shallow vadose zone is made up by six soil layers (0–0.05, 0.05–0.15, 0.15–0.30, 0.30–0.60, 0.60–1.0, and 1–2 m delimited by the horizontal solid lines in the blue rectangle). Water flow in the shallow vadose zone is described by the Richards equation that requires the net precipitation (P), obtained by subtracting rainfall intercepted by vegetation from gross precipitation measured by the weather station, and biome-specific potential evapotranspiration, ET_p, as boundary forcings. ET_p is split into potential evaporation (E_p) and potential transpiration (T_p) by using a time-variant leaf area index obtained from remote-sensing products. Other important input data are root zone depth (D_{rz}) and soil hydraulic properties (SHPs). The output data include actual evaporation (E_a), actual transpiration (T_a), water storage (WS), and GR_p.

The soil moisture from GR_p travels through the deep unsaturated vadose zone and becomes GR_a at the water table depth (D_{wt}) after a delay (or lag time, τ). It is apparent from the calculations of water mass conservation that the GR rate will not change if there are no impeding soil layers between the root zone and the aquifer (Zlotnik et al., 2007; Rossman et al., 2014). The time to reach the water table is calculated by using a simplified physically based equation defined by the depth to the water table, soil moisture profile, and soil hydraulic parameters. This time may vary on the scale from years to many centuries (Rossman et al., 2014; Dandekar et al., 2018).

Setup of HYDRUS-1D in the Shallow Vadose Zone

HYDRUS-1D is a public-domain Windows-based model used for simulating water, heat, and solute movement across the vadose zone (Šimunek et al., 2016). HYDRUS-1D solves the Richards equation for describing water flow in unsaturated or fully saturated porous media:

$$\frac{\partial \theta}{\partial t} = \frac{\partial}{\partial z}\left[K\left(\psi\right)\left(\frac{\partial \psi}{\partial z} + 1\right)\right] - S \tag{1}$$

where t is time expressed in units of days (d), ψ is the pressure head (m), z is the soil depth (positive upward) (m), θ is the volumetric soil water content (m^3 m^{-3}), and S is the sink term (d^{-1}) describing the actual plant root water extraction rate function depending on z, ψ, and the potential transpiration (T_p).

The soil water retention function, $\theta\left(\psi\right)$ is described by van Genuchten's equation denoted here as VG for brevity (van Genuchten, 1980):

$$\theta\left(\psi\right) = \theta_r + \frac{\theta_s - \theta_r}{\left[1 + \left(\alpha_{VG}\psi^n\right)\right]^m} \tag{2}$$

where α_{VG} (m^{-1}), m (–), and n (–) are water retention shape parameters, and θ_r (m^3 m^{-3}) and θ_s (m^3 m^{-3}) are residual and saturated water contents, respectively.

Parameters m and n are related as follows: $m = 1–1/n$ (Mualem, 1976). Considering the degree of saturation, $S_e = (\theta-\theta_r)/(\theta_s-\theta_r)$, which varies from 0 ($\theta = \theta_r$) to 1 ($\theta = \theta_s$), the unsaturated hydraulic conductivity function, $K(S_e)$ is given by the following equation:

$$K\left(S_e\right) = K_s S_e^l \left[1 - \left(1 - S_e^{1/m}\right)^m\right]^2 \tag{3}$$

where K_s (m d^{-1}) is the saturated hydraulic conductivity, and l is the tortuosity parameter that is assumed to be 0.5 (Mualem, 1976).

The upper boundary condition depends on fluxes occurring at the soil surface (namely P and E_p). Gross precipitation P_g is intercepted by vegetation; thus, rainfall interception I_R has been calculated as shown in the following equation (Nasta and Gates, 2013):

$$I_R = aLAI(1 - \frac{1}{1 + \frac{bP_g}{aLAI}}) \qquad (4)$$

where a (m d^{-1}) is an empirical coefficient, assumed as 0.00025 m d^{-1}, and b (–) denotes the soil cover fraction given by

$$b = 1 - e^{-kLAI} \qquad (5)$$

where κ is a dimensionless extinction coefficient for global solar radiation inside the canopy and is assumed to be equal to 0.463. Interception is subtracted from P_g to obtain the net rainfall P that has been calculated in study locations and used as input in HYDRUS-1D.

ET_p is calculated by multiplying ET_0 by a dimensionless biome-specific coefficient, K_c (i.e., $ET_p = ET_0 \times K_c$). The LAI is also used to partition ET_p into E_p and T_p using the following equation (Ritchie, 1972):

$$E_P = ET_p e^{-\kappa LAI} \qquad (6)$$

Potential transpiration (T_p), corresponding to potential root water uptake, is obtained by subtracting E_p from ET_p. K_c and LAI are time-variant and change daily (Batsukh et al., 2021). The root distribution is assumed to be linear in the soil profile and spans from 1 (corresponding to the maximum root density) at the soil surface to 0 (corresponding to the minimum root density) at the root zone bottom.

The sink term, S, is defined as the actual plant root water extraction rate function (Feddes et al., 1978):

$$S(\psi) = \alpha_F(\psi)T_p \qquad (7)$$

where $\alpha_F(\psi)$ is a piecewise linear function ($0 \leq \alpha_F(\psi) \leq 1$) depending on prescribed pressure head values for describing the root-water uptake water stress (de Melo and de Jong van Lier, 2021). HYDRUS-1D provides tabulated values for ψ depending on plant characteristics. In this study, pasture was selected as a suitable plant in Mongolia.

The lower boundary condition is set to free drainage (unit vertical hydraulic gradient). Information on initial soil moisture or matric potential profile at the beginning of the numerical simulation is unavailable (Yu et al., 2019). Thus, the initial condition was set with the soil moisture results from model spin-ups.

PTFs have been widely used to predict soil hydraulic parameters in favor of expensive laboratory or field measurements (Schaap et al., 2001; Zhang and Schaap, 2017). Most PTFs estimate VG parameters of empirical hydraulic

functions with modest accuracy (Zhang and Schaap, 2017), when available from generalized regional data. The Rosetta PTF, built into the HYDRUS-1D and based on artificial neural network analysis, is used for the estimation of the soil hydraulic parameters in this study.

Calculation of Lag Time in the Deep Vadose Zone

Drainage rates in thick unsaturated zones rarely reflect current fluxes or recharge rates at the water table (Scanlon et al., 2002). Annual average drainage in HYDRUS-1D in the top 2-m-thick soil layer is assumed equal to GR_p traveling from control volume bottom (D_{cv}=2 m) to the water table depth (D_{wt}). The assumption is made that the soil moisture profile in the deep vadose zone is uniform, which is characteristic for semi-arid regions with a stable climate, e.g., in the High Plains in the USA as observed by McMahon et al. (2006). Then, vadose zone lag time can be calculated using the water table depth and soil moisture vertical velocity (c) according to Zlotnik et al. (2007) and Rossman et al. (2014). The equation for calculating c is obtained using the traveling wave solution of the Richards equation and can be expressed for VG soil properties in Equations 1 and 2 as follows:

$$c = \frac{dK(\theta)}{d\theta} = \frac{K_s(1 - S_f^m)^2}{2(\theta_s - \theta_r)S_e^{1/2}}[1 + \frac{4S_e^{1/m}S_f^{m-1}}{(1 - S_f^m)}] \qquad (8)$$

where S_f is:

$$S_f = 1 - S_e^{1/m} \qquad (9)$$

Once c has been determined from Equation 8, the lag time τ can be computed as follows:

$$\tau = (D_{wt} - D_{cv})/c \qquad (10)$$

Evaluation Criteria and Statistical Analysis

Datasets of water balance components obtained in HYDRUS-1D are summarized through basic indices of descriptive statistics such as mean ($\bar{x}$), standard deviation (sd), coefficient of variation (CV), minimum (min), and maximum (max). Student's t-test is applied to estimate the population mean of P, ET_0, ET_p, AI, E_a, T_a, and GR_p; the sample mean is used when the population standard deviation is unknown. Student's t-distribution is used to construct the 95% confidence interval ($\alpha = 0.05$) around the sample mean in each emission scenario to infer the population mean (μ):

$$\mu = \bar{x} \pm t_{\alpha, n-1} \frac{sd}{\sqrt{n}} \qquad (11)$$

where n is the number of weather stations (degrees of freedom are therefore defined as n-1), and $t_{\alpha,n-1}$ is Student's t-value at 95% confidence interval and n-1 degrees of freedom. To measure the predictive capability of all prediction methods, we selected two statistical performance indicators: the root mean square error (RMSE), which combines both bias and lack of precision, and the

coefficient of determination (R^2), which measures how well the data pairs fit to a line:

$$RMSE = \sqrt{\frac{1}{n}\sum_{i=1}^{n}(o_i - e_i)^2} \qquad (12)$$

$$R^2 = \frac{\sum_{i=1}^{n}(o_i - e_i)^2}{\sum_{i=1}^{n}(o_i - \overline{o})^2} \qquad (13)$$

where o_i is the reference value, $\overline{o}$ is the mean of reference values, and e_i indicates values modeled by the prediction method. The subscript i is the index of the weather stations, and n is the total number of stations ($n = 41$).

Partial least-squares regression (PLSR) is a statistical method for analyzing the complex interaction of a large array of predictors and the dependent variable (Wold et al., 2001; Carrascal et al., 2009). PLSR is an extension of the multiple linear regression model for which the dependent variable (y) is predicted by a set of predictors (x) as follows:

$$y = \beta_0 + \beta_1 x_1 + \beta_2 x_2 + \ldots + \beta_p x_p \qquad (14)$$

where β_0 is the regression coefficient for the intercept, β_i is the i-th regression coefficient, and p is the total number of predictor variables. PLSR was used to define the explained variance of GR_p and τ patterns by exploiting soil–climate–vegetation factors as predictor variables. Soil proxy data are the percentages of sand, silt, and clay contents, and bulk density, as well as the depth to water table. Climate data are FAO aridity index (AI), whereas the available land cover auxiliary variable considered in this study is the annual-average leaf area index (LAI) retrieved from freely available remote-sensing products. This technique generates new components as linear combinations of the original predictor variables. PLSR finds combinations of the predictors that have a large covariance with the dependent variable. The predictive ability of the PLSR will be expressed in terms of R^2 and $RMSE$, which evaluate the scatter of the data points around the identity line and the bias between PLSR-based and composite model simulated GR_p and τ values. In the PLSR modeling, the importance of a predictor is indicated by the variable importance in the projection (VIP) (Yan et al., 2013). The factors with high VIP values of more than 1 are the most relevant in explaining the dependent variable and are considered to be significantly influential predictors. Wold (1995) suggests that those predictors with VIP > 0.8 are the most relevant for explaining the dependent variable, and those with VIP < 0.5 are considered to be of minor importance for the prediction of the dependent variable. It is thus possible to determine those environmental factors (predictor variables) that strongly interact with GR_p and τ (the dependent variables).

RESULTS

Assessment of Potential Groundwater Recharge Rates in the Shallow Vadose Zone

GR_p simulated in HYDRUS-1D depends on climate forcings (P, E_p, and T_p), soil hydraulic parameters (SHPs) in each soil layer,

root depth (D_{rz}), root vertical distribution, initial conditions in terms of soil moisture, and prescribed pressure head values controlling the Feddes reduction factor (α_F). Due to lack of information, the last three factors were kept constant over the 41 experimental sites in Mongolia. In contrast, the first three factors characterizing climate, soil, and vegetation influence the numerical simulations in HYDRUS-1D and the spatial variability of output data. As done in Batsukh et al. (2021), we considered the numerical simulations in two (Sukhbaatar, Arvaikheer) sites in the steppe region and one site (Saikhanovoo) in the Gobi Desert (**Figure 2**). The three sites are characterized by contrasting climate and vegetation cover with maximum (Sukhbaatar), average (Arvaikheer), and minimum (Saikhanovoo) AI and annual-average LAI values in Mongolia (**Table 1**).

The numerical simulations of cumulative P, cumulative ET_a, WS, and cumulative GR_p can be visualized in **Figure 2**. The mean annual GR_p in Saikhanovoo (Gobi Desert) is similar to the one simulated in Arvaikheer (steppe region). Mean annual precipitation ($P = 113$ mm year^{-1}) and actual evapotranspiration ($ET_a = 99.7$ mm year^{-1}) fluxes in Saikhanovoo are half those in Arvaikheer ($P = 219$ mm year^{-1} and $ET_a = 202$ mm year^{-1}). T_a represents 11 and 19% of ET_a in Saikhanovoo and Arvaikheer, respectively. This is reflected in average WS values of 382 and 415 mm. The mean annual GR_p in Saikhanovoo and Arvaikheer is higher than the mean annual GR_p in Sukhbaatar with a higher-than-normal P in Mongolia ($P = 277$ mm year^{-1}). Nevertheless, the higher-than-normal vegetation cover in Sukhbaatar induces high actual transpiration fluxes (51% of ET_a) occurring during the rainy season by reducing WS (296 mm < WS < 387 mm corresponding to vertical-average soil water content of 0.148 m^3 m^{-3} < θ < 0.194 m^3 m^{-3}) and consequently GR_p.

Table 2 shows the sample mean ($\overline{x}$), standard deviation (sd), coefficient of variation (CV), minimum (min), and maximum (max) of soil physical (sand, silt, clay, bulk density) and soil hydraulic parameters (θ_r, θ_s, α_{VG}, n, K_s) for the six functional layers over the 41 weather stations. The soil physical properties (sand, silt, clay, bulk density) downloaded from SoilGrids250m are quite uniform in space as depicted by their CV that is lower than 15%. The soil physical parameters are implemented in Rosetta PTF to obtain the soil hydraulic parameters featuring in the water retention function (Equation 2) and in the hydraulic conductivity function (Equation 3). The low spatial variability of SHPs is contrasted by the high spatial variability of annual-average LAI (Batsukh et al., 2021).

The descriptive statistics of mean annual water balance components, namely gross precipitation (P_g), rainfall interception (I_R), grass-reference potential evapotranspiration (ET_0), biome-specific potential evapotranspiration (ET_p), actual evapotranspiration (ET_a), and potential groundwater recharge (GR_p), simulated in HYDRUS-1D over the 41 weather stations are reported in **Table 3**.

The spatial-average mean annual P_g and ET_0 are about 180 and 860 mm year^{-1}, respectively. Precipitation spans between 56.6 and 323 mm year^{-1} and therefore is characterized by relevant spatial variability ($CV = 43\%$) while ET_0 is spatially quite uniform. By using a time-variant crop coefficient adapted for Mongolia, we report a relevant reduction of ET_0 into ET_p
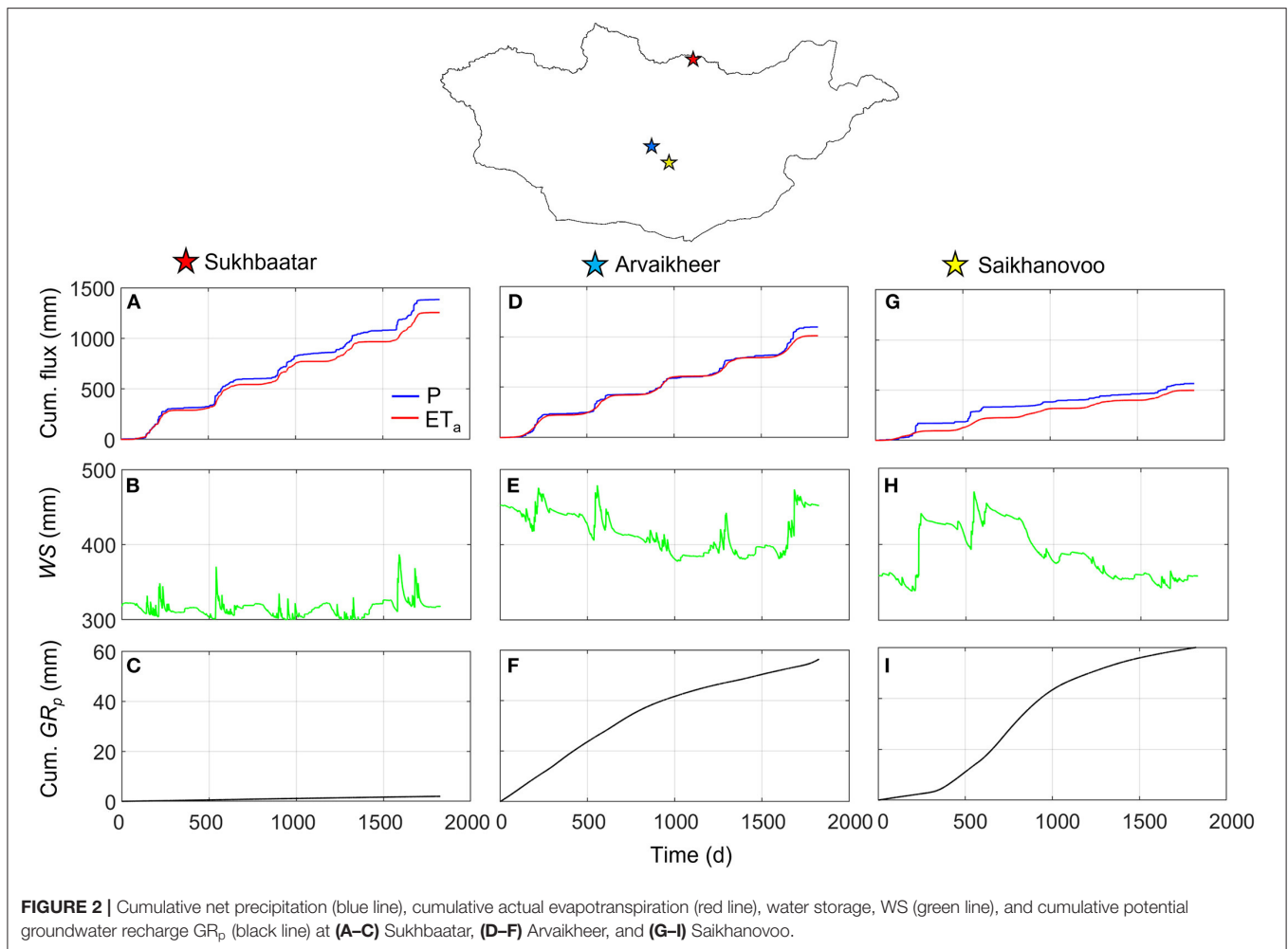
FIGURE 2 | Cumulative net precipitation (blue line), cumulative actual evapotranspiration (red line), water storage, WS (green line), and cumulative potential groundwater recharge GR$_p$ (black line) at **(A–C)** Sukhbaatar, **(D–F)** Arvaikheer, and **(G–I)** Saikhanovoo.

(Batsukh et al., 2021). The population mean (μ) values of ET_a and GR_p range between 151 and 184 and 2.5 and 4.0 mm year^{-1}, respectively. ET_a represents the main water balance component simulated in HYDRUS-1D and on average ET_a constitutes more than 95% of rainfall. Runoff was zero in all numerical simulations over the 41 study locations as the soil is dry during most of the year (Banzragch and Shinoda, 2011).

We point out that, according to Batsukh et al. (2021), 29 stations belong to the steppe region where spatial-average mean annual P and ET_0 are about 213 and 810 mm year^{-1}, respectively, resulting in semi-arid climate ($AI = 0.27$). The remaining 12 stations belong to the Gobi Desert, where spatial-average mean annual P and ET_0 are about 97 and 974 mm year^{-1}, respectively, resulting in $AI = 0.10$, which corresponds to the arid climate. ET_p/ET_0 is on average 50 and 20% in the steppe and Gobi Desert, respectively. T_p/ET_p is on average 30 and 11% in the steppe and Gobi Desert, respectively.

The simulations of the water balance in HYDRUS-1D report the following outcomes. In the steppe region, spatially averaged mean annual E_a, T_a, and GR_p are 130, 61, and 3.3 mm year^{-1}, respectively. On average ET_a and GR_p represent 94 and 1.7% of P,

respectively. In the Gobi Desert, spatially averaged mean annual E_a, T_a, and GR_p are 77, 14, and 3.8 mm year^{-1}, respectively. On average, $ET_a/P = 94\%$ is similar, while $GR_p/P = 3.5\%$ doubles if compared to the values reported for the steppe region. On average T_a is 33% of ET_a in steppe regions with higher LAI, while it decreases toward the Gobi region where E_a constitutes from 71 to 89% of ET_a.

The model simulations were tested with values reported in the available maps. The simulated mean annual ET_a values were compared to those reported in the FAO map (**Figure 3A**). **Figure 3B** shows the relationship between mapped and simulated mean annual ET_a values by reporting $RMSE = 59.3$ mm year^{-1} and $R^2 = 0.61$. This relatively high discrepancy is due to underestimation in seven locations, especially in the steppe region in northern Mongolia.

The simulated mean annual GR_p values are compared to the values reported in the Renewable Groundwater Resources map (**Figure 4A**). We observe fair agreement only in the class at the lowest GR_p values (<5 mm year^{-1}) over 20 weather stations (**Figure 4B**). In all other classes, we report a significant

underestimation of GR_p, especially in classes with the highest GR_p values (10–300, 50–100, and 100–200 mm year^{-1}).

These results can be compared quantitatively in more detail by analyzing the effect of environmental controls on mean annual GR_p values (Yin et al., 2017). We used the PLSR

approach to assess soil–climate–vegetation controlling factors (bulk density, sand, silt, clay, LAI, and AI) (**Figure 5**). The PLSR automatically generates six new components, which reproduce mean annual GR_p patterns with $R^2 = 0.53$, $RMSE = 2.3$ mm year^{-1}, and an explained variability of 47.1%. However, the match with the identity line (1:1 line) is consistent up to $GR_p = 8$ mm year^{-1}, but it deteriorates for greater values. GR_p

TABLE 1 | Climate annual mean variables (ET_0, P, AI, ET_p, E_p, T_p), soil physical (D_{rz}, D_{wt}, BD, clay, silt, sand), and hydraulic (θ_s, θ_r, α_{VG}, n, K_s) parameters and vegetation characteristics (LAI) at Sukhbaatar, Arvaikher, and Saikhanovoo experimental sites.

|	Unit	Sukhbaatar	Arvaikheer	Saikhanovoo
ET_0	mm year^{-1}	852.3	803.7	962.6
P	mm year^{-1}	276.8	219.4	113.2
AI	–	0.325	0.273	0.118
LAI	–	0.98	0.24	0.14
ET_p	mm year^{-1}	694.9	227.6	147.1
E_p	mm year^{-1}	329.1	186.8	134.0
T_p	mm year^{-1}	365.8	40.8	13.0
D_{rz}	m	0.30	0.30	0.30
D_{wt}	m	10	15	15
BD	kg m^{-3}	1447	1476	1473
Clay	%	23.00	23.31	21.04
Silt	%	28.32	35.79	36.82
Sand	%	48.68	40.90	42.15
θ_s	m^3 m^{-3}	0.43	0.41	0.40
θ_r	m^3 m^{-3}	0.067	0.066	0.063
α_{VG}	m^{-1}	1.368	1.068	1.061
n	–	1.45	1.49	1.50
K_s	m d^{-1}	0.231	0.129	0.115

TABLE 2 | Statistics of soil physical and hydraulic properties for six functional layers over the 41 weather stations.

|	BD	Clay	Silt	Sand	θ_s	θ_r	α_{VG}	n	K_s	D_{wt}
	kg m^{-3}	%	%	%	m^3 m^{-3}	m^3 m^{-3}	m^{-1}	–	m d^{-1}	m
$\bar{x}$	1,457	23.60	35.40	41.00	0.417	0.068	1.096	1.49	0.16	14.0
sd	31	2.95	4.09	3.55	0.016	0.005	0.176	0.037	0.05	10.1
CV	2.09	12.50	11.56	8.67	3.80	7.21	16.06	2.50	32.80	72.5
Min	1,383	18.58	24.75	34.26	0.392	0.058	0.838	1.38	0.08	5.0
Max	1,524	33.03	42.38	48.68	0.460	0.081	1.550	1.55	0.32	52.0

TABLE 3 | Statistics of the water balance components simulated in HYDRUS-1D over the 41 weather stations.

	P_g	I_R	ET_0	ET_p	ET_a	GR_p
	mm year^{-1}	mm year^{-1}	mm year^{-1}	mm year^{-1}	mm year^{-1}	mm year^{-1}
$\bar{x}$	178.8	7.8	858.0	309.0	167.3	3.2
SD	76.8	6.0	108.9	139.0	71.0	3.4
CV	43.0	77.8	12.7	45.0	42.5	103.5
Min	56.6	26.4	633.6	125.8	54.0	0.3
Max	322.5	1.3	1,128.6	694.9	297.6	12.0
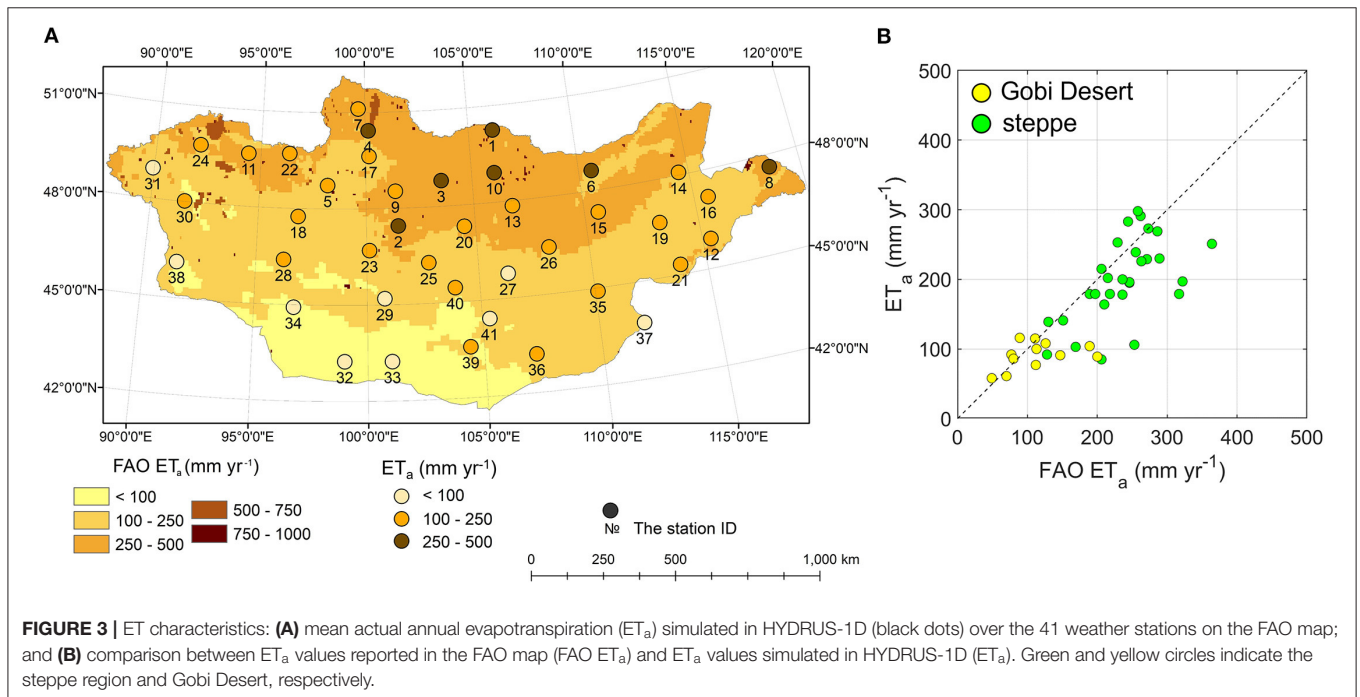
FIGURE 3 | ET characteristics: **(A)** mean actual annual evapotranspiration (ET_a) simulated in HYDRUS-1D (black dots) over the 41 weather stations on the FAO map; and **(B)** comparison between ET_a values reported in the FAO map (FAO ET_a) and ET_a values simulated in HYDRUS-1D (ET_a). Green and yellow circles indicate the steppe region and Gobi Desert, respectively.
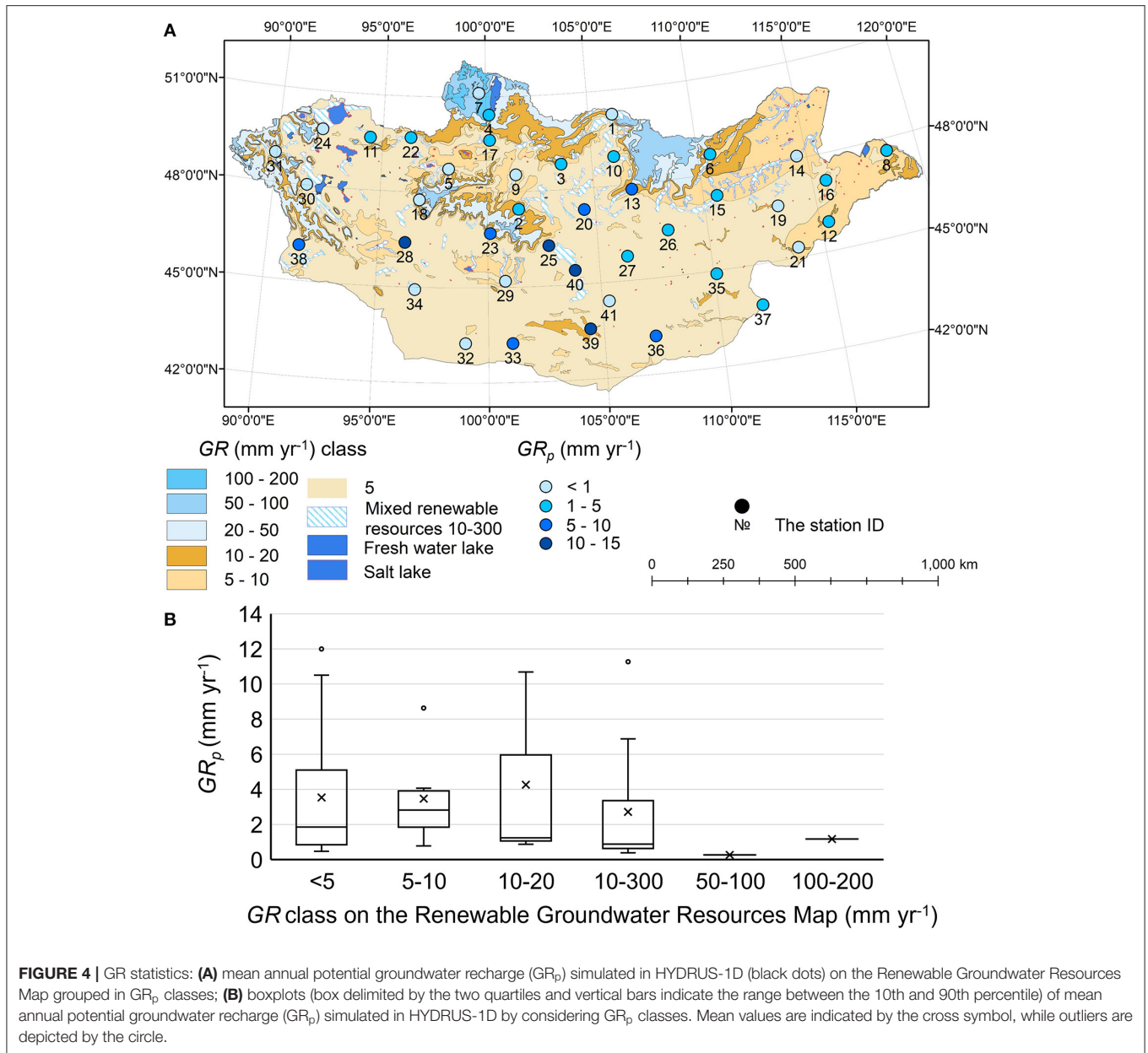
FIGURE 4 | GR statistics: **(A)** mean annual potential groundwater recharge (GR$_p$) simulated in HYDRUS-1D (black dots) on the Renewable Groundwater Resources Map grouped in GR$_p$ classes; **(B)** boxplots (box delimited by the two quartiles and vertical bars indicate the range between the 10th and 90th percentile) of mean annual potential groundwater recharge (GR$_p$) simulated in HYDRUS-1D by considering GR$_p$ classes. Mean values are indicated by the cross symbol, while outliers are depicted by the circle.
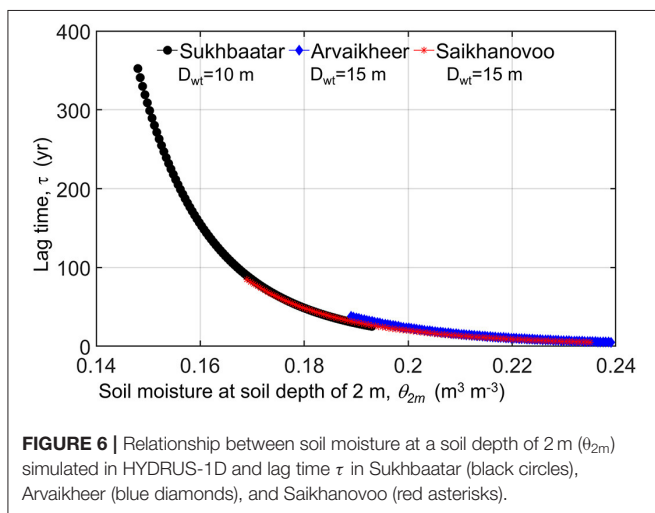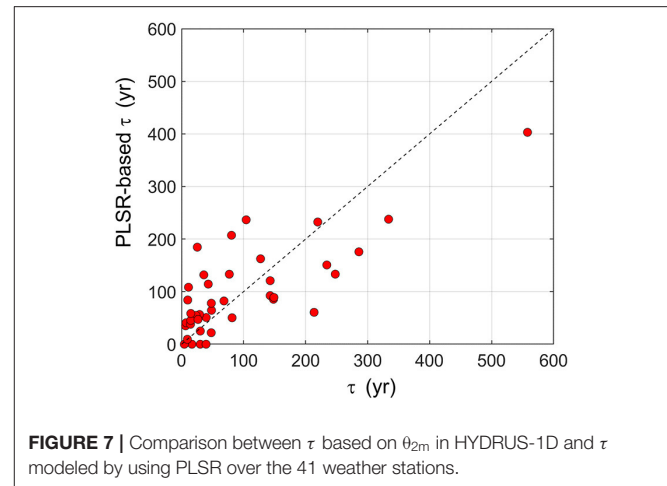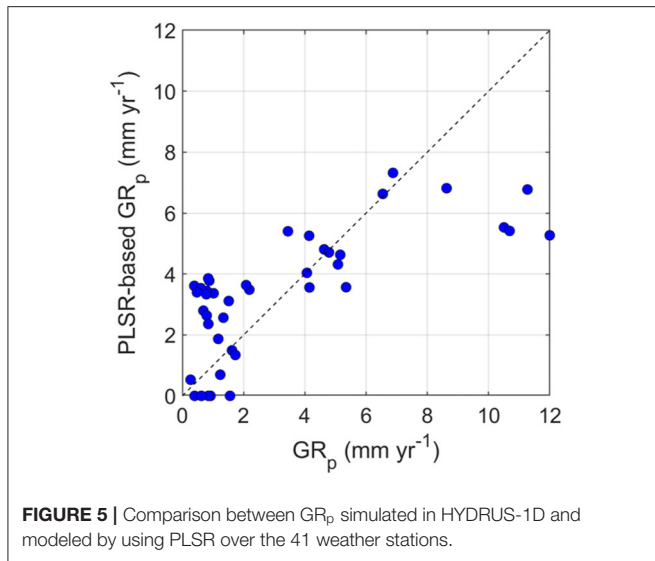
values higher than 8 mm year^{-1} are underestimated by PLSR-modeled estimates. The variable importance in the projection (VIP) of each explanatory variable helps indicate the most important predictors in explaining the spatial variability of GR$_p$. By considering a total of six components (the same number of predictor variables), clay, *LAI*, and *AI* are the most important predictors with VIP>0.8 while the least relevant ones are bulk density and sand content with VIP of 0.22 and 0.49, respectively.

Few studies use PLSR for explaining the spatial variability of GR$_p$. Shawul et al. (2019) found that land cover classes are able to explain more than 90% of *GR* at catchment scale in a PLSR analysis carried out in Ethiopia. Most studies use PLSR analysis to detect those environmental factors controlling near-surface soil

moisture or other water balance components (Huang et al., 2015; Li et al., 2017).

Assessment of Lag Time in the Deep Vadose Zone

Once the GR$_p$ values are simulated in HYDRUS-1D, the lag time τ can be calculated from soil moisture vertical velocity (c), depth to the water table (D_{wt}), and depth of control volume (D_{cv}) in Equation 10. While D_{wt} and D_{cv} are known, soil moisture featuring in the degree of saturation S_e in Equation 10 is unknown. Therefore, we assume that soil moisture at the soil depth of 2 m (θ_{2m}) at the end of the numerical simulation is equal to the soil moisture across the deep soil profile (D_{wt}–D_{cv}) by crudely ignoring its vertical variation. Therefore, a
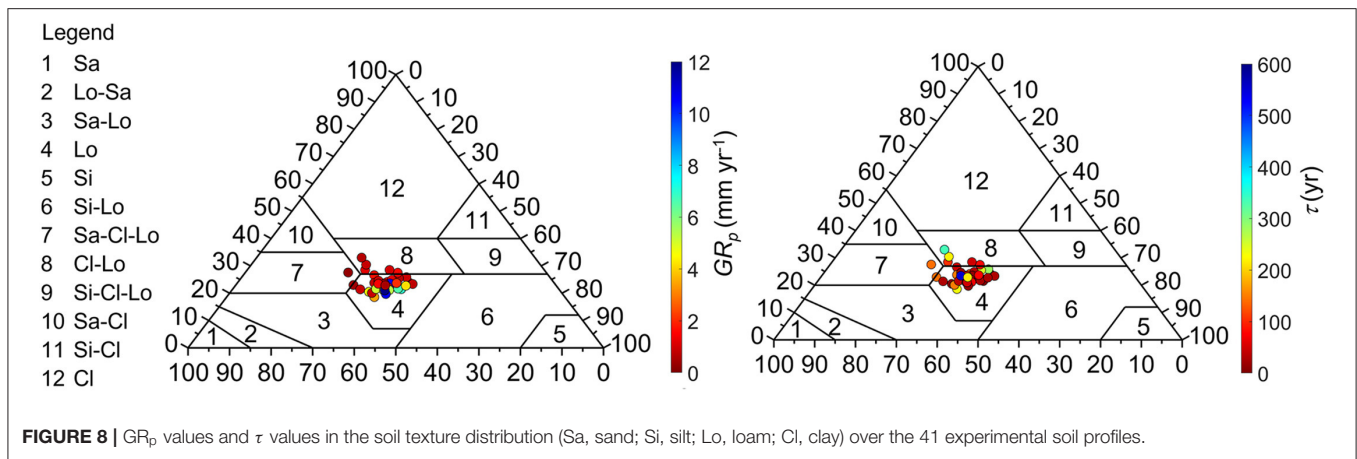
FIGURE 5 | Comparison between GR$_p$ simulated in HYDRUS-1D and modeled by using PLSR over the 41 weather stations.

FIGURE 6 | Relationship between soil moisture at a soil depth of 2 m (θ_{2m}) simulated in HYDRUS-1D and lag time τ in Sukhbaatar (black circles), Arvaikheer (blue diamonds), and Saikhanovoo (red asterisks).

sensitivity analysis of τ-values to the soil moisture profile is highly recommended (**Figure 6**). In doing so, we calculate the lag time (Equation 10) depending on the soil water content at the soil depth of 2 m in Sukhbaatar (0.148 m^3 m^{-3} < θ_{2m} < 0.194 m^3 m^{-3}), Arvaikheer (0.189 m^3 m^{-3} < θ_{2m} < 0.239 m^3 m^{-3}), and Saikhanovoo (0.169 m^3 m^{-3} < θ_{2m} < 0.235 m^3 m^{-3}). **Figure 6** shows that the lag time is highly sensitive to soil moisture simulated in HYDRUS-1D. The lag time decays exponentially between 25.3 and 352.3 years in Sukhbaatar, between 5.2 and 37.8 years Arvaikheer, and between 5.2 and 84.6 years Saikhanovoo. Therefore, a small change in soil moisture might influence the lag time by two orders of magnitude, and this indicates the paramount importance of numerical simulations in the shallow vadose zone.

The lag times calculated over the 41 experimental sites span between 4.4 and 557.8 years with spatial-average τ of 92.5 years. We analyzed the predictive ability of the five soil controlling factors (bulk density, sand, silt, clay, depth to water table) to

FIGURE 7 | Comparison between τ based on θ_{2m} in HYDRUS-1D and τ modeled by using PLSR over the 41 weather stations.

explain the spatial variability of τ. To do so, the PLSR was used, and the results are illustrated in **Figure 7**. The comparison between τ simulated in HYDRUS-1D and modeled with the PLSR is expressed using the R^2, $RMSE$, and explained variance by using five components that are fairly able to reproduce τ patterns with $R^2 = 0.61$, and explained variability of 59.1%. $RMSE = 71.69$ years indicates a large uncertainty. According to the VIP values, the most important contributors are depth to the water table and silt with VIP = 1.88 and VIP = 0.86, respectively. Bulk density is the least relevant factor in explaining the spatial variability of τ by reporting VIP = 0.37. The PLSR results highlight the relevant importance of assessing the depth to water table and silt as key predictors for travel time in Mongolia.

DISCUSSION

Groundwater modeling requires aquifer properties (hydraulic conductivity, thickness of saturated zone, specific yield, storage coefficient), lateral boundary conditions, and rates of groundwater recharge GR_a and withdrawals. Nonetheless, obtaining this set of input data is time-consuming and expensive, especially in data-poor countries under arid and semi-arid conditions (Scanlon et al., 2006). It is apparent that over a vast territory such as Mongolia, the magnitude of the diffuse recharge compared to focused recharge from surface water–groundwater interactions varies significantly due to the diversity of hydrologic conditions, and previously such estimates were entirely missing. Therefore, our results are not applicable in areas with extensive surface water–groundwater interactions. The diffuse GR_p depends on the climate, water table depth, soil hydraulic properties of the vadose zone, and vegetation characteristics influencing evapotranspiration fluxes. It is very difficult to characterize the soil hydraulic properties of layered soil profiles throughout large-scale domains. In this study, only information on soil physical properties within the top 2 m of the vadose zone was used to simulate water fluxes in HYDRUS-1D. The Rosetta PTF was employed in six soil layers to retrieve five unknown soil hydraulic parameters (θ_r, θ_s, α_{VG}, n, K_s)

FIGURE 8 | GR_p values and τ values in the soil texture distribution (Sa, sand; Si, silt; Lo, loam; Cl, clay) over the 41 experimental soil profiles.

describing the soil water retention and hydraulic conductivity functions. Other existing PTFs developed for large datasets could be tested as well (Nasta et al., 2021; Weihermüller et al., 2021). Nonetheless, the SoilGrids250m database provides soil texture data distributed mainly in the following classes: clay loam, sandy clay loam, and loam. The mean annual GR_p values depicted using the USDA texture triangle (**Figure 8**) are lower than $2\,\mathrm{mm\,year^{-1}}$ (reddish color) in the sandy clay loam and clay loam classes and are variable in the loam class. In contrast, lag time τ tends to be lower than 100 years in the loam class, with some exceptions.

Estimating all of the water balance components of the vadose zone is the key to providing a robust assessment of diffuse GR. This recharge is the residual amount of water moving to the water table after the water losses of actual evapotranspiration and runoff. Topography was ignored in this study, and we assumed one-dimensional independent soil columns for 41 experimental soil profiles (Cuthbert et al., 2019).

We observed weak sensitivity of the mean annual precipitation–recharge relationship in Mongolia, which is supported by some studies in similar regions (Deng et al., 2015; Huang et al., 2017). Soil moisture profiles across the vadose zone under permanent dry conditions simulated in HYDRUS-1D induce weak sensitivity of mean annual GR_p to precipitation supply. Therefore, it is unfeasible to obtain simple empirical relationships as done in other parts of the world (Crosbie et al., 2010; Cuthbert et al., 2019).

The substantial role of recharge resulting from surface water–groundwater interactions clearly can explain higher values of GR in topographic depressions occupied by streams and wetlands with runoff from mountainous areas. The effects of the accumulation and snowmelt on recharge were ignored as well (Small, 2005).

Vegetation characteristics were provided in terms of LAI retrieved from freely available remote-sensing products (Mao and Yan, 2019). LAI is used to quantify rainfall interception, the partition of ET_p into E_p and T_p, which are crucial steps for obtaining reliable numerical simulations in HYDRUS-1D (Kool et al., 2014; Anderson et al., 2017; Lama et al., 2021). Vegetation influences evapotranspiration that decreases exponentially with

decreasing root depth (Adane et al., 2018). The role of vegetation characteristics in assessing ET_p was already considered by Batsukh et al. (2021). The validation of ET_a values simulated in HYDRUS-1D with those reported in the FAO-map corroborates the acceptable prediction capability. In New Mexico and Nevada, Gee et al. (1994) found that water percolated in vegetation-free deep lysimeters, whereas percolation did not occur in lysimeters with growing vegetation. Recharge is generally much greater in non-vegetated than in vegetated regions (Gee et al., 1994) and greater in areas with annual crops and grasses than in areas with perennial plant such as trees and shrubs (Prych, 1998; Scanlon et al., 2002; Adane et al., 2018). According to our results, GR_p is lower in areas with denser vegetation as well as in areas with deeper root systems. Desert vegetation such as the shrub Larrea (Creosote bush) has relatively deep root systems (David and Vokhmin, 2002), and it transpires until the soil water pressure reaches the wilting point ($\psi > 810.00\,\mathrm{m}$) (Pockman and Sperry, 2000). GR_p values in two of our study locations that are covered by shrubs with deep root systems are lower than those simulated in other study locations in the Gobi Desert. More detailed studies on the plant-specific uptake parameters in Mongolia are needed in the future for improving model simulations.

The Renewable Groundwater Resource Map representing diffuse and local GR is practically the only published material that can be used for indirect inference of groundwater recharge in Mongolia. Our results are consistent with the map: the renewable groundwater resources on the map are greater than simulated GR rates, especially in large river catchments as well as within the mountain ranges. The prediction of GR_p in the study locations presented in this paper have similar results in surrounding regions such as Inner Mongolia, China (e.g., Huang and Pang, 2013; Huang et al., 2017). According to Huang et al. (2017), the diffuse recharge beneath the grassland is 0.11–$0.32\,\mathrm{mm\,year^{-1}}$, based on the chloride mass balance over seven soil profiles. On the other hand, according to Huang and Pang (2013), recharge in the northwestern part of China is commonly $<3.6\,\mathrm{mm\,year^{-1}}$, where precipitation is $<200\,\mathrm{mm\,year^{-1}}$, and groundwater is mainly recharged by mountain runoff. The recharge rates increase in the rainfed Loess Plateau, ranging from 30 to $100\,\mathrm{mm\,year^{-1}}$ beneath the main crop represented by

wheat. An average recharge rate of 1.4 mm year^{-1} is also found by Gates et al. (2008) in Badain Jaran Desert in northwestern China. These studies indicate that the groundwater recharge decreases toward the arid grassland steppe in China. According to our study, GR_p does not typically exceed 12 mm year^{-1} in Mongolia without an additional irrigation supply. Our results are validated by groundwater observations, although uncertainties are still substantial (Taylor et al., 2013; Sood and Smakhtin, 2015; Turkeltaub et al., 2015).

Groundwater recharge occurs as water percolates through overlying unsaturated zones to become stored in an aquifer system. Determining the lag time for the vadose zone is critical for quantifying groundwater renewable resources and water quality (Jasechko, 2019). Some progress in the calibration of process-based models using isotope-based techniques (Stumpp et al., 2012; Sprenger et al., 2016; Boumaiza et al., 2020) has been published recently.

We have collated a basic data archive to feed physically based models for estimating GR over a limited number of locations in Mongolia and short time series of daily weather data (a 5-year-long dataset). The ever-increasing availability of input data from other archives and potential field studies will increase the reliability of analyses.

CONCLUSIONS

We present the first study explicitly estimating the diffuse GR in Mongolia by using a composite physically based model approach. Previously, the GR concept and analyses for water resource evaluations were underutilized in Mongolia.

Results provide diffuse GR in 41 locations of Mongolia at the spatial resolution of about 200 km × 200 km by using climate data for the 2007–2011 period. Estimates utilize easily accessible databases for weather data (precipitation and biome-specific potential evapotranspiration), soil physical properties (bulk density, sand, silt, clay), and freely available remote-sensing products for vegetation characteristics (leaf area index). Acquisition of key input data might further enhance model performance. PLSR analysis identifies the most important contributors in explaining the spatial variability of GR and τ.

In Mongolia, the diffuse GR rates are very low compared to precipitation in all locations, with an annual mean of <12 mm year^{-1} in all considered study locations. ET_a is the most relevant water balance component that was verified by available FAO data.

Our results on GR values in most regions of Mongolia are consistent with the Renewable Groundwater Resource map that is based on hydrograph separation, while it shows differences in river watersheds, topographic depressions, and other areas of focused recharge. This comparison is also consistent with GR composition, which includes both diffuse recharge and localized recharge due to the surface water–groundwater interactions. Among future topics, research should evaluate the impact of climate, land use, and land cover changes on water balance components of the vadose zone, including GR and lag time. Verification of results can be assessed by setting up ground-truth measurements in representative locations for the steppe region and the Gobi Desert.

DATA AVAILABILITY STATEMENT

The original contributions presented in the study are included in the article/**Supplementary Material**, further inquiries can be directed to the corresponding author/s.

AUTHOR CONTRIBUTIONS

All authors listed have made a substantial, direct, and intellectual contribution to the work and approved it for publication.

FUNDING

ACKNOWLEDGMENTS

SUPPLEMENTARY MATERIAL

The Supplementary Material for this article can be found online at: https://www.frontiersin.org/articles/10.3389/frwa.2022.802208/full#supplementary-material

REFERENCES

Adane, Z. A., Nasta, P., Zlotnik, V., and Wedin, D. (2018). Impact of grassland conversion to forest on groundwater recharge in the Nebraska Sand Hills. *J. Hydrol.* 15, 171–183. doi: 10.1016/j.ejrh.2018.01.001

Anderson, R. G., Zhang, X., and Skaggs, T. H. (2017). Measurement and partitioning of evapotranspiration for application to Vadose Zone studies. *Vadose Zone J.* 16, 1–9. doi: 10.2136/vzj2017.08.0155

Banzragch, N., and Shinoda, M. (2011). Seasonal change of soil moisture in Mongolia: its climatology and modelling. *Int. J. Climatol.* 31, 1143–1152. doi: 10.1002/joc.2134

Batsukh, K., Zlotnik, V. A., Suyker, A., and Nasta, P. (2021). Prediction of biome-specific potential evapotranspiration in mongolia under a scarcity of weather data. *Water* 13:2470. doi: 10.3390/w13182470

Bayanzul, B., Nakamura, K., Machida, I., Watanabe, N., and Komai, T. (2019). Construction of a conceptual model for confined groundwater flow in the Gunii

Khooloi Basin, Southern Gobi Region, Mongolia. *Hydrogeol. J.* 27, 1581–1596. doi: 10.1007/s10040-019-01955-8

Boumaiza, L., Chesnaux, R., Walter, J., and Stumpp, C. (2020). Constraining a flow model with field measurements to assess water transit time through a Vadose Zone. *Ground Water* 59:13056. doi: 10.1111/gwat.13056

Carrascal, L. M., Galván, I., and Gordo, O. (2009). Partial least squares regression as an alternative to current regression methods used in ecology. *Oikos* 118, 681–690. doi: 10.1111/j.1600-0706.2008.16881.x

Crosbie, R., Scanlon, B., Mpelasoka, F., Reedy, R., Gates, J., and Zhang, L. (2013). Potential climate change effects on groundwater recharge in the High Plains Aquifer, USA. *Water Resour. Res.* 49, 3936–3951. doi: 10.1002/wrcr.20292

Crosbie, R. S., Jolly, I. D., Leaney, F. W., and Petheram, C. (2010). Can the dataset of field based recharge estimates in Australia be used to predict recharge in data-poor areas? *Hydrol. Earth Syst. Sci.* 14, 2023–2038. doi: 10.5194/hess-14-2023-2010

Cuthbert, M. O., Taylor, R. G., Favreau, G., Todd, M. C., Shamsudduha, M., Villholth, K. G., et al. (2019). Observed controls on resilience of groundwater to climate variability in sub-Saharan Africa. *Nature* 572, 230–234. doi: 10.1038/s41586-019-1441-7

Dandekar, A. T., Singh, D. K., Sarangi, A., and Singh, A. K. (2018). Modelling vadose zone processes for assessing groundwater recharge in semi-arid region. *Curr. Sci.* 114, 608–618. doi: 10.18520/cs/v114/i03/608-618

David, F. H., and Vokhmin, V. (2002). The global biogeography of roots. *J. Nucl. Sci. Technol.* 39, 286–289. doi: 10.1080/00223131.2002.10875464

de Melo, M. L. A., and de Jong van Lier, Q. (2021). Revisiting the Feddes reduction function for modeling root water uptake and crop transpiration. *J. Hydrol.* 603, 126952. doi: 10.1016/j.jhydrol.2021.126952

Deng, L., Wang, W., Cai, Y., Hu, A., and Tan, L. (2015). Groundwater diffuse recharge and its response to climate changes in semi-arid northwestern China. *Terrestr. Atmos. Ocean. Sci.* 26, 451–461. doi: 10.3319/TAO.2015.03.18.01(Hy)

Doble, R. C., and Crosbie, R. S. (2017). Revue: Méthodes courantes et émergentes pour la modélisation de la recharge à l'échelle du bassin versant et de l'évapotranspiration d'eaux souterraines peu profondes. *Hydrogeol. J.* 25, 3–23. doi: 10.1007/s10040-016-1470-3

FAO (2009). *Global Map of Yearly Actual ET*. Retrieved from: https://data.apps.fao.org/map/catalog/srv/eng/catalog.search#/home (accessed November 17, 2020).

Feddes, R. A., Kowalik, P. J., and Zaradny, H. (1978). *Simulation of Field Water Use and Crop Yield*. Wageningen : Centre for Agricultural Publishing and Documentation. Retrieved from: http://lib.ugent.be/catalog/rug01:000032129

Gates, J. B., Edmunds, W. M., Ma, J., and Sheppard, P. R. (2008). A 700-year history of groundwater recharge in the drylands of NW China. *Holocene* 18, 1045–1054. doi: 10.1177/0959683608095575

Gee, G. W., Wierenga, P. J., Andraski, B. J., Young, M. H., Fayer, M. J., and Rockhold, M. L. (1994). Variations in water balance and recharge potential at three western desert sites. *Soil Sci. Society of Am. J.* 58, 63–72. doi: 10.2136/sssaj1994.03615995005800010009x

Gombo, D., and Dambaravjaa, O. (2012). *Part 1. Surface Water Resources Assessment - Integrated Water Management National Assessment Report Volume I*. Ulaanbaatar, Mongolia.

Healy, R. W. (2011). *Estimating Groundwater Recharge*. Cambridge University Press. doi: 10.1017/CBO9780511780745

Hengl, T., de Jesus, J., Heuvelink, G. B. M., Ruiperez Gonzalez, M., Kilibarda, M., Blagotić, A., et al. (2017). SoilGrids250m: global gridded soil information based on machine learning. *PLoS ONE* 12, e0169748. doi: 10.1371/journal.pone.0169748

Huang, T., and Pang, Z. (2013). Groundwater recharge and dynamics in Northern China: implications for sustainable utilization of groundwater. *Proc. Earth Planet. Sci.* 7, 369–372. doi: 10.1016/j.proeps.2013.03.182

Huang, T., Pang, Z., Liu, J., Yin, L., and Edmunds, W. M. (2017). Groundwater recharge in an arid grassland as indicated by soil chloride profile and multiple tracers. *Hydrol. Proc.* 31, 1047–1057. doi: 10.1002/hyp.11089

Huang, X., Shi, Z.-H., Zhu, H. D., Zhang, H., Lei, A., and Yin, W. (2015). Soil moisture dynamics within soil profiles and associated environmental controls. *Catena* 136, 14. doi: 10.1016/j.catena.2015.01.014

Indree, T. (2014). *The Steppe Vegetation of Mongolia*. Ulaanbaatar. Retrieved from: https://www.researchgate.net/publication/271448082_The_Steppe_Vegetation_of_Mongolia

Jadambaa, N., Batjargal, D., Linden, W., van der, Batsukh, N., and Borchuluun, U. (2012). *Part 4. Groundwater Resources Assessment in Integrated Water Management - National Assessment Report Volume I*. Ulaanbaatar. Retrieved from: http://bic.iwlearn.org/en/documents/documents/state-reports/2012/integrated-water-management-natioinal-report-volume-i-english/view

Jasechko, S. (2019). Global isotope hydrogeology—review. *Rev. Geophys.* 57, 835–965. doi: 10.1029/2018RG000627

Jyrkama, M. I., Sykes, J. F., and Normani, S. D. (2002). Recharge estimation for transient ground water modeling. *Ground Water* 40, 638–648. doi: 10.1111/j.1745-6584.2002.tb02550.x

Kool, D., Agam, N., Lazarovitch, N., Heitman, J. L., Sauer, T. J., and Ben-Gal, A. (2014). A review of approaches for evapotranspiration partitioning. *Agric. Forest Meteorol.* 184, 56–70. doi: 10.1016/j.agrformet.2013.09.003

Lama, G. F. C., Giovannini, M. R. M., Errico, A., Mirzaei, S., Padulano, R., Chirico, G. B., et al. (2021). Hydraulic efficiency of green-blue flood control scenarios for vegetated rivers: 1D and 2D unsteady simulations. *Water.* 13, 2620. doi: 10.3390/w13192620

Lerner, D., Issar, A. S., and Simmers, I. (1990). Groundwater recharge: a guide to understanding and estimating natural recharge. *J. Environ. Qual.* 21, 345. doi: 10.2134/jeq1992.00472425002100030036x

Li, S. G., Asanuma, J., Kotani, A., Davaa, G., and Oyunbaatar, D. (2007). Evapotranspiration from a Mongolian steppe under grazing and its environmental constraints. *J. Hydrol.* 333, 133–143. doi: 10.1016/j.jhydrol.2006.07.021

Li, Z., Xu, X., Xu, C., Liu, M., Wang, K., and Yu, B. (2017). Annual runoff is highly linked to precipitation extremes in Karst catchments of Southwest China. *J. Hydrometeorol.* 18, 2745–2759. doi: 10.1175/JHM-D-17-0032.1

Mao, J., and Yan, B. (2019). *Global Monthly Mean Leaf Area Index Climatology, 1981-2015*. Oak Ridge, TN: ORNL DAAC.

McMahon, P. B., Dennehy, K. F., Bruce, B. W., Böhlke, J. K., Michel, R. L., Gurdak, J. J., et al. (2006). Storage and transit time of chemicals in thick unsaturated zones under rangeland and irrigated cropland, High Plains, United States. *Water Resourc. Res.* 42:4417. doi: 10.1029/2005WR004417

Meixner, T., Manning, A. H., Stonestrom, D. A., Allen, D. M., Ajami, H., Blasch, K. W., et al. (2016). Implications of projected climate change for groundwater recharge in the western United States. *J. Hydrol.* 534, 124–138. doi: 10.1016/j.jhydrol.2015.12.027

Mineral Resources and Petroleum Authority (1994). *Hydrogeology Map 1:500000*. Mineral resources and Petreloum Authority, Ulaanbaatar, Mongolia.

Mualem, Y. (1976). A new model for predicting the hydaulic conductivity of unsaturated porous media. *Water Res. Res.* 12, 513. doi: 10.1029/WR012i003p00513

Nandintsetseg, B., Shinoda, M., Kimura, R., and Ibaraki, Y. (2010). Relationship between soil moisture and vegetation activity in the Mongolian steppe. *Sci. Online Lett. Atmos.* 6, 29–32. doi: 10.2151/sola.2010-008

Nasta, P., and Gates, J. B. (2013). Plot-scale modeling of soil water dynamics and impacts of drought conditions beneath rainfed maize in Eastern Nebraska. *Agric. Water Manag.* 128, 120–130. doi: 10.1016/j.agwat.2013.06.021

Nasta, P., Szabó, B., and Romano, N. (2021). Evaluation of pedotransfer functions for predicting soil hydraulic properties: a voyage from regional to field scales across Europe. *J. Hydrol.* 37, 100903. doi: 10.1016/j.ejrh.2021.100903

Pockman, W., and Sperry, J. (2000). Vulnerability to xylem cavitation and the distribution of Sonoran desert vegetation. *Am. J. Botany* 87, 1287–1299. doi: 10.2307/2656722

Pozdniakov, S. P., Vasilevsky, P. Y., Grinevskiy, S. O., Lekhov, V. A., Sizov, N. E., and Wang, P. (2020). Variability in spatial-temporal recharge under the observed and projected climate: a site-specific simulation in the black soil region of Russia. *J. Hydrol.* 590, 125247. doi: 10.1016/j.jhydrol.2020.125247

Prych, E. A. (1998). *Using Chloride and Chlorine-36 as Soil-Water Tracers to Estimate Deep Percolation at Selected Locations on the US Department of Energy Hanford Site*. Washington, DC: US Geological Survey.

Regional Hydrogeologic Map of Mongolia, Multi-year Mean Flow of Surface Water and Groundwater (1981). Aerogeology Research Institute, Moscow, Soviet Union.

Ritchie, J. T. (1972). Model for predicting evaporation from a row crop with incomplete cover. *Water Resourc. Res.* 8, 1204–1213. doi: 10.1029/WR008i005p01204

Rossman, N. R., Zlotnik, V. A., Rowe, C. M., and Szilagyi, J. (2014). Vadose zone lag time and potential 21st century climate change effects on spatially distributed groundwater recharge in the semi-arid Nebraska Sand Hills. *J. Hydrol.* 519, 656–669. doi: 10.1016/j.jhydrol.2014.07.057

Scanlon, B., Healy, R., and Cook, P. (2002). Choosing appropriate techniques for quantifying groundwater recharge. *Hydrogeol. J.* 10, 18–39. doi: 10.1007/s10040-001-0176-2

Scanlon, B. R., Keese, K. E., Flint, A. L., Flint, L. E., Gaye, C. B., Edmunds, W. M., et al. (2006). Global synthesis of groundwater recharge in semiarid and arid regions. *Hydrol. Proc.* 20, 3335–3370. doi: 10.1002/hyp.6335

Schaap, M. G., Leij, F. J., and Van Genuchten, M. T. (2001). Rosetta: a computer program for estimating soil hydraulic parameters with hierarchical pedotransfer functions. *J. Hydrol.* 251, 163–176. doi: 10.1016/S0022-1694(01)00466-8

Shawul, A., Chakma, S., and Melesse, A. (2019). The response of water balance components to land cover change based on hydrologic modeling and partial least squares regression (PLSR) analysis in the Upper Awash Basin. *J. Hydrol.* 26, 100640. doi: 10.1016/j.ejrh.2019.100640

Šimunek, J., van Genuchten, M. T., and Šejna, M. (2016). Recent developments and applications of the HYDRUS computer software packages. *Vadose Zone J.* 15, 33. doi: 10.2136/vzj2016.04.0033

Small, E. E. (2005). Climatic controls on diffuse groundwater recharge in semiarid environments of the southwestern United States. *Water Resourc. Res.* 41, 1–17. doi: 10.1029/2004WR003193

Sood, A., and Smakhtin, V. (2015). Revue des modèles hydrologiques globaux. *Hydrol. Sci. J.* 60, 549–565. doi: 10.1080/02626667.2014.950580

Spinoni, J., Vogt, J., Naumann, G., Carrao, H., and Barbosa, P. (2015). Towards identifying areas at climatological risk of desertification using the Köppen-Geiger classification and FAO aridity index. *Int. J. Climatol.* 35, 2210–2222. doi: 10.1002/joc.4124

Sprenger, M., Seeger, S., Blume, T., and Weiler, M. (2016). Travel times in the vadose zone: Variability in space and time. *Water Resourc. Res.* 52, 5727–5754. doi: 10.1002/2015WR018077

Stumpp, C., Stichler, W., Kandolf, M., and Šimunek, J. (2012). Effects of land cover and fertilization method on water flow and solute transport in five lysimeters: a long-term study using stable water isotopes. *Vadose Zone J.* 11:75. doi: 10.2136/vzj2011.0075

Taylor, R. G., Scanlon, B., Döll, P., Rodell, M., Van Beek, R., Wada, Y., et al. (2013). Ground water and climate change. *Nat. Clim. Change* 3, 322–329. doi: 10.1038/nclimate1744

Turkeltaub, T., Kurtzman, D., Bel, G., and Dahan, O. (2015). Examination of groundwater recharge with a calibrated/validated flow model of the deep vadose zone. *J. Hydrol.* 522, 618–627. doi: 10.1016/j.jhydrol.2015.01.026

van den Bosch, R., and Batjes, N. H. (2013). *ISRIC - World Soil Information (WDC-Soils).* Ulaanbaatar: Ministry of Environment and Tourism.

van Genuchten, M. T. (1980). A closed-form equation for predicting the hydraulic conductivity of unsaturated soils. *Soil Sci. Society Am. J.* 44, 892–898. doi: 10.2136/sssaj1980.03615995004400050002x

Wang, T., Zlotnik, V. A., Šimunek, J., and Schaap, M. G. (2009). Using pedotransfer functions in vadose zone models for estimating groundwater recharge in semiarid regions. *Water Resourc. Res.* 45, 1–12. doi: 10.1029/2008WR006903

Wang, Z. Y., Hou, J., Qu, Z. Q., Guo, J. Y., and Li, J. R. (2017). Root distribution of 430 plants in temperate grassland of northern China. *Appl. Ecol. Environ. Res.* 15, 1625–1651. doi: 10.15666/aeer/1503_16251651

WaterGAP 2.1, University of Frankfurt/Main; modified by WHYMAP, B. (2008). *Mean Annual Groundwater Recharge for the WMO Standard Hydrological Period 1961-1990.* Retrieved from: https://www.whymap.org/whymap/EN/Maps_Data/Gwv/gw_recharge_g.html;nn$=$9930678 (accessed May 10, 2021).

Weihermüller, L., Lehmann, P., Herbst, M., Rahmati, M., Verhoef, A., Or, D., et al. (2021). Choice of pedotransfer functions matters when simulating soil water balance fluxes. *J. Adv. Model. Earth Syst.* 13, 2404. doi: 10.1029/2020MS002404

Wold, S. (1995). *PLS for Multivariate Linear Modeling. Chemometric Methods in Molecular Design*, 195–218. Retrieved from: http://ci.nii.ac.jp/naid/10031086076/en/

Wold, S., Sjöström, M., and Eriksson, L. (2001). PLS-regression: a basic tool of chemometrics. *Chemometr. Intel. Lab. Syst.* 58, 109–130. doi: 10.1016/S0169-7439(01)00155-1

Yan, B., Fang, N. F., Zhang, P. C., and Shi, Z. H. (2013). Impacts of land use change on watershed streamflow and sediment yield: an assessment using hydrologic modelling and partial least squares regression. *J. Hydrol.* 484, 26–37. doi: 10.1016/j.jhydrol.2013.01.008

Yanagawa, A., Fujimaki, H., Okuro, T., Jamsran, U., and Takeuchi, K. (2015). Comparison of drought tolerances in a root water uptake model for two co-occurring grass species in Mongolia. *J. Jpn. Soc. Soil Phys.* 130, 3–10.

Yembuu, B. (1906). The physical geography of Mongolia: Ulaanbaatar, Mongolia. *Nature* 74. doi: 10.1038/074527a0

Yin, L., Hou, G., Huang, J., Li, Y., Wang, X., Yang, Z., et al. (2011). "Using chloride mass-balance and stream hydrographs to estimate groundwater recharge in the Hailiutu River Basin, NW China," in *ISWREP 2011–Proceedings of 2011 International Symposium on Water Resource and Environmental Protection, vol. 1* (Piscataway, NJ: IEEE), 325–328.

Yin, Z., Feng, Q., Yang, L., Wen, X., Si, J., and Zou, S. (2017). Long term quantification of climate and land cover change impacts on streamflow in an alpine river catchment, northwestern China. *Sustainability* 9, 1278. doi: 10.3390/su9071278

Yu, D., Yang, J., Shi, L., Zhang, Q., Huang, K., Fang, Y., et al. (2019). On the uncertainty of initial condition and initialization approaches in variably saturated flow modeling. *Hydrol. Earth Syst. Sci.* 23, 2897–2914. doi: 10.5194/hess-23-2897-2019

Yu, W., Wu, T., Wang, W., Li, R., Wang, T., Qin, Y., et al. (2016). Spatiotemporal changes of reference evapotranspiration in Mongolia during 1980-2006. *Adv. Meteorol.* 2016, 1–14. doi: 10.1155/2016/9586896

Zhang, Y., and Schaap, M. G. (2017). Weighted recalibration of the Rosetta pedotransfer model with improved estimates of hydraulic parameter distributions and summary statistics (Rosetta3). *J. Hydrol.* 547, 39–53. doi: 10.1016/j.jhydrol.2017.01.004

Zlotnik, V. A., Wang, T., Nieber, J., and Šimunek, J. (2007). Verification of numerical solutions of the Richards equation using a traveling wave solution. *Adv. Water Resour.* 30, 1973–1980. doi: 10.1016/J.Jhydrol.2015.12.019

Zlotnik, V. A., Ward, A. S., Harvey, J. W., Lautz, L. K., Rosenberry, D. O., and Brunner, P. (2016). "Groundwater-surface water interactions," in *The Handbook of Groundwater Engineering: Third Edition*, eds J. Cushman and D. Tartakovsky (Boca Raton, FL: CRC Press), 237–288. doi: 10.1201/9781315371801-10